Volume 1 | Number 1 | Jan 2013 | Pages 1–100

Dalton Transactions

An international journal of inorganic chemistry
www.rsc.org/dalton

ROYAL SOCIETY
OF CHEMISTRY

ROYAL SOCIETY
OF CHEMISTRY

www.rsc.org/dalton

Journal Name

Dalton Transactions

Dynamic Article Links ▶

ARTICLE TYPE

Diverse Structures of Metal – Organic Frameworks Based on Different Metal Ions: Luminescence and Gas Adsorption Properties

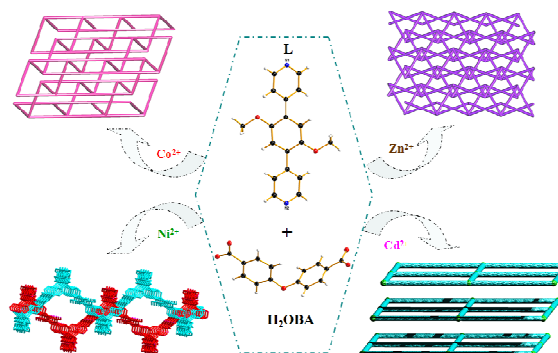**Chuan-Lei Zhang, Ling Qin, Zhen-Zhen Shi and He-Gen Zheng***

Four coordination polymers with different metal ions have been synthesized based on a rigid linear pyridine and a flexible V-shaped dicarboxylate ligand (L = 4,4'-(2,5-dimethoxy-1,4-phenylene)dipyridine; H_2OBA = 4,4'-oxydibenzoic acid): $\{[Co(L)(OBA)]\cdot2H_2O\}_n$ (**1**), $[Zn(L)(OBA)\cdot2H_2O]_n$ (**2**), $\{[Ni(L)(OBA)]\cdot DMF\cdot H_2O\}_n$ (**3**), $[Cd(L)(OBA)]\cdot DMF\cdot H_2O\}_n$ (**4**). The reaction conditions are similar

10 except metal ions for complexes **1-4**. Complexes **1** and **2** present a 3D unprecedented **hxg-d-4-*Cccm*** net, but **3** and **4** are 4-connected **sql** nets with point symbol $\{4^4\cdot6^2\}$. These complexes have been characterized by single crystal X-ray diffraction, infrared spectroscopy, thermogravimetry, elemental analysis, and powder X-ray diffraction measurements. UV–visible spectra, Fluorescence and gas adsorption properties of the compounds have also been explored.

Introduction

15   Because of the fantastic chemical and physical properties, the design and synthesis of metal–organic frameworks is still quite active for scientists and engineers.[1-5] Over the past few decades, one great effort is devoted to the design and synthesis of new

20 organic ligands as well as their effects on the structures and properties of metal–organic frameworks.[6] Another important endeavor is to understand the impact of different metal ions in coordination polymers. Coordination polymers based on N-donor and polycarboxylate ligands have received considerable attention

25 because they can incorporate virtues of different functional groups and it is easier to get architecture controlled by changing one of the above two kinds of ligands.[7] Rigid ligands for its desired geometry and stable skeleton, have been used to design specific topologies. Flexible ligands can bend and rotate when

30 coordinate to metal centers, resulting in the structural diversity of coordination polymers.[8] More and more complexes assembled by the same ligand with different metal ions have appeared in literature.[9] But, the comparative study on the assembly process of the same ligands influenced by different metal ions, either similar

35 metal series like spherical d^{10} cations (Zn^{2+} and Cd^{2+}),[10] or distinct ionic size and electronic configurations of metal cations (e.g., Co^{2+}, Ni^{2+} and Zn^{2+}), has been seldom investigated in details.[11]

    In previous work, we employed 4,4'-(2,5-dimethoxy-1,4-

40 phenylene) dipyridine and 2',5'-dimethoxy-[1,1':4',1"-terphenyl]-4,4"-dicarboxylic acid as ligands to construct coordination polymers. We found that the matching of reactants will influence structures of coordination polymers.[1] In order to further investigate the effects of metal ions on structures in a certian

45 mixligand system, 4,4'-(2,5-dimethoxy-1,4-phenylene) dipyridine and 4,4'-oxydibenzoic acid as well as Co^{2+}, Ni^{2+}, Zn^{2+} and Cd^{2+} were chosen (Scheme 1). In this paper, four coordination polymers based on M(II) (M = Co, Ni, Zn, Cd) have been successfully prepared and characterized by single crystal X-ray

50 diffraction, infrared spectroscopy, thermogravimetry, elemental analysis, and powder X-ray diffraction measurements. Fluorescence and gas adsorption properties of the compounds have also been explored.

State Key Laboratory of Coordination Chemistry, School of Chemistry and Chemical Engineering, Collaborative Innovation Center of Advanced Microstructures, Nanjing University, Nanjing 210093 (P. R. China)
Fax: (+86)25-83314502,
E-mail: zhenghg@nju.edu.cn

55 Scheme 1. Schematic representation of structures diversity caused by different metal ions.

Dalton Transactions Accepted Manuscript

Results and discussion

The experimental section has been listed in the Supporting Information. The detailed information of complexes **1-4** is summarized in Table 1 and S1.

Description of the crystal structure of {[Co(L)(OBA)]·2H$_2$O}$_n$ (1) and [Zn(L)(OBA)·2H$_2$O]$_n$ (2)

Single-crystal structure analysis reveals that **1** and **2** are isomorphous and crystallize in the monoclinic crystal system with *C*2/*c* space group. Hence, only the structure of **1** is described in detail and the structure description of crystal **2** can be found in the Supporting Information (Figure S16). The asymmetric unit of **1** contains one Co(II) metal center, two halves L ligands, one OBA^{2-} anion and two lattice water molecules squeezed by PLATON software.[13] Each Co(II) is coordinated by two nitrogen atoms from two nearly vertical L ligands and two carboxylate oxygen atoms from two OBA^{2-} ligands (nearly in a line), which forms tetrahedral coordination configuration (Figure 1a). The Co–O bond distances are 1.9752(14) and 1.9771(15) Å, and the Co–N bond distances are 2.0521(15) and 2.0542(15) Å; the O–Co–O angle is 106.04(7)°, N–Co–N angle is 102.99(6)°, and the N–Co–O angles are in the range of 93.92(6)–129.90(7)°. There are two types of chains in the structure, one *zig–zag* chain is formed by L ligands and Co(II) cation centers containing a Co⋯Co distance of 15.4679(10) Å and a Co–Co–Co angle of 104.822(2)°, the other chain is constructed from OBA^{2-} ligands and Co(II) cations, the Co⋯Co distance is 14.1230(8) Å (Figure 1b). Such 1D *zig–zag* chains are linked by the other chains in the tilting direction, leading to the formation of a 3D framework (Figure 1c).

A better insight into the nature of this intricate framework can be achieved by the application of a topological approach, reducing multidimensional structures to simple nodes and connection nets. The Co centers can be regarded as 4-connected nodes and all crystallographical independent L and OBA^{2-} ligands acted as linkers. Thus, the whole structure can thus be represented as a **hxg-d-4-*Cccm*** net with the point symbol of {6^5·8} (Figure 1d). From the latest CCDC upgrade package (UpdateFeb14), it has been reported rarely with the subnet of **hxg-d-4** topology,[14] the **hxg-d-4-*Cccm*** topology is the first case of **hxg** type. Removal of the guest molecules creates a void volume of 701.8 Å^3 (11.3% of the unit cell volume). Compared with other weaving structures, this whole 3D framework has no interpenetration for its low porosity.
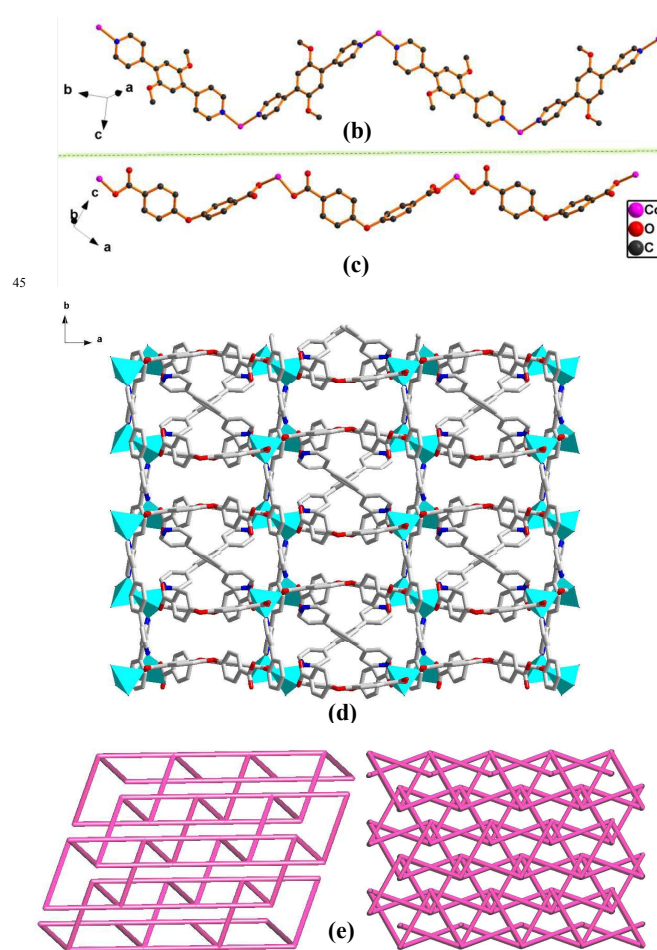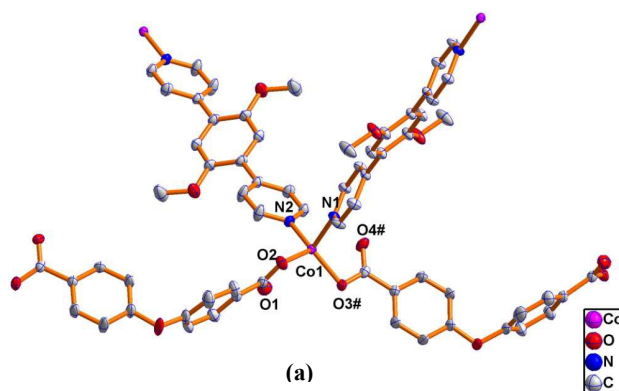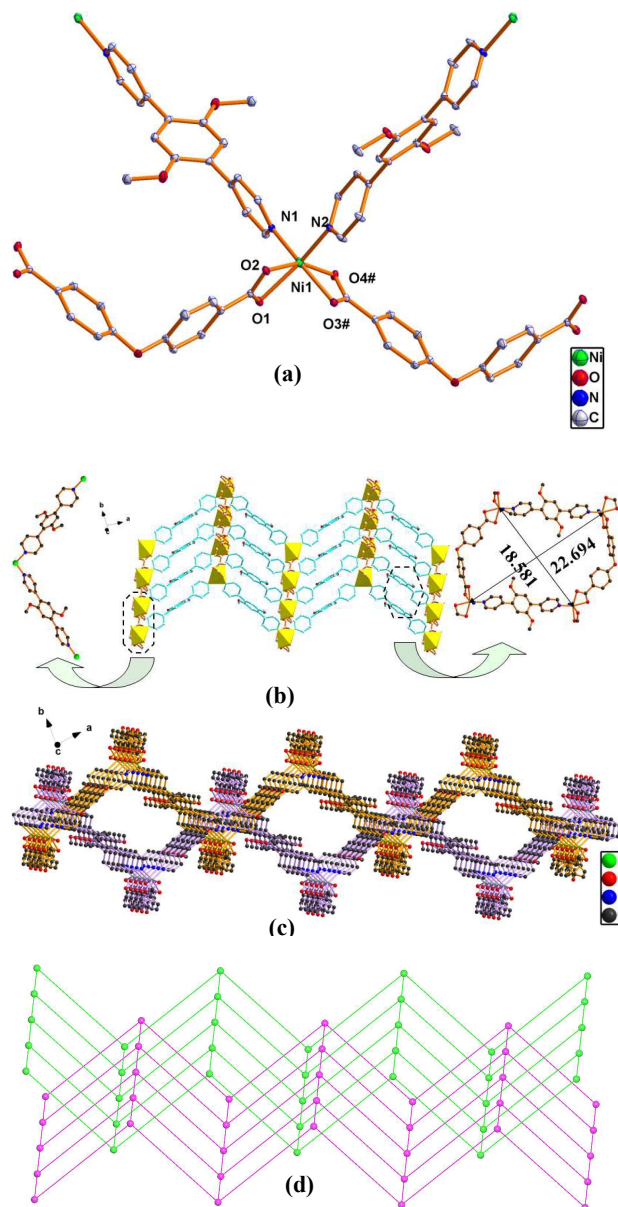

Figure 1. (a) Coordination environment of the Co(II) ion in **1**. The hydrogen atoms are omitted for clarity (30% ellipsoid probability). Symmetry codes: # 0.5 + *x*, 0.5 − *y*, 0.5 + *z*; (b) *Zig-zag* chain formed by L ligands and Co(II) cations and (c) *Zig-zag* chain constructed from OBA^{2-} ligands and Co(II) ions; (d) Polyhedral representation of the 3D framework of **1**; (e) Views of **hxg-d-4-*Cccm*** topology (left, *b*-axis; right, (111) plane) of **1**.

Description of the crystal structure of {[Ni(L)(OBA)]·DMF·H$_2$O}$_n$ (3)

X-ray diffraction reveals that complex **3** crystallizes in the triclinic crystal system of *P*1̄ space group. Its asymmetric unit consists of one Ni(II) ion, two halves L ligands, one OBA^{2-} ligand, one solvent DMF and one water molecule (Figure 2a). The Ni(II) is defined by two almost vertical L ligands and four carboxylate oxygen atoms from two OBA^{2-} ligands, in a seriously distorted octahedral geometry with Ni–O bond distances between 2.0457(19) and 2.232(2) Å, Ni–N bond distances 2.031(2) and 2.048(2) Å, N–Ni–N angle 96.12(9)°, N–Ni–O angles between 89.86(8) and 161.57(8)°, and O–Ni–O angles between 61.94(7)–157.24(9)°. OBA^{2-} ligands adopt bidentate chelating mode to combine Ni (II) ions to form 1D chains. Another *zig–zag* chains constructed by L ligands and Ni (II) ions cross the above chains to form a 2D wave-like layer (Figure 2b). This undulating (4, 4) network possesses the rhomb-like windows with diagonal size about 18.581 × 22.694 Å^2. The large enough rhomboid voids of each layer allow one layer to interpenetrate with another in a parallel interpenetrated 2D+2D→2D architecture (Figure 2c and

2d). After interpenetrating, the solvent-accessible volume is 314.9 $Å^3$ or 19.7% of the total unit cell volume, calculated with the PLATON program. These voids are occupied by DMF and H_2O solvent molecules, which have been crystallographically [5] identified and well refined.

(a)
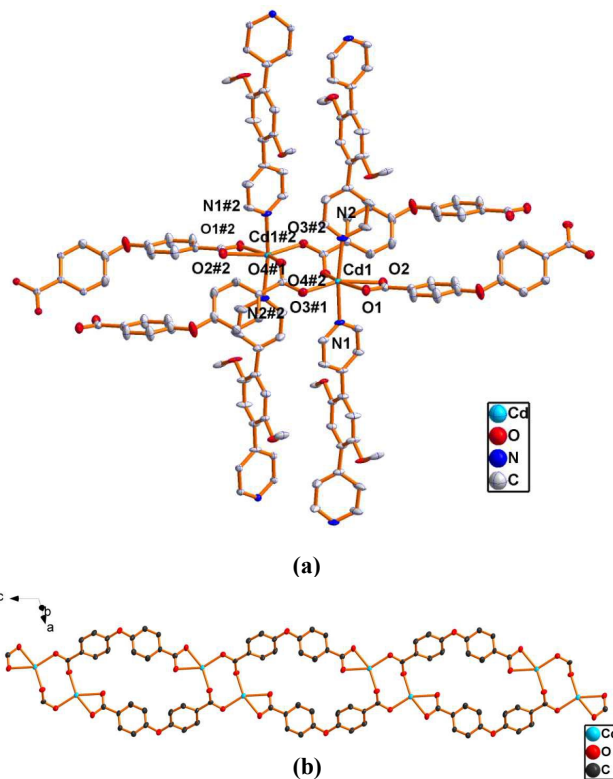

(b)

(c)

(d)

[10] Figure 2. (a) Coordination environment of the Ni(II) ion in **3**. The hydrogen atoms and solvent molecules are omitted for clarity (30% ellipsoid probability). Symmetry codes: #1 = x, y, $1 + z$; (b) The wave-like layer of **3** (left: 1D chain constructed from OBA^{2-} ligands and Ni^{2+} ions, right: the rhomb-like window with diagonal size about 18.581 × 22.694 [15] $Å^2$); (c) Parallel interpenetrated architecture of 2D + 2D→2D and (d) topological representation of the **sql** net.

Description of the crystal structure of {[Cd(L)(OBA)]·DMF·H₂O}ₙ (4)

Complex **4** also displays a 2D structure and crystallizes in the [20] triclinic crystal system of $P\bar{1}$ space group. The asymmetric unit of **4** consists of one Cd(II) ion, one L ligand, one OBA^{2-} ligand, one

solvent DMF and one water molecule squeezed by PLATON software. Each Cd(II) ion is coordinated by four carboxylate oxygen atoms from three different OBA^{2-} ligands and two [25] nitrogen atoms from two L ligands, which adopt octahedral coordination modes (Figure 3a). Two carboxyl groups of OBA^{2-} ligand adopt two different coordination modes, one adopt bidentate bridging node to combine two Cd(II) ions, the other adopt bidentate chelating mode to chelate one Cd(II) ion. Pairs of [30] Cd(II) cations are joined by two symmetrical OBA^{2-} ligands to generate a dinuclear $Cd_2(CO_2)_2$ secondary building unit (SBU) with a Cd···Cd separation of 4.519(11) Å. These $Cd_2(CO_2)_2$ SBUs are further bridged through the second symmetrical OBA^{2-} ligands into a 1D chain with a loop (Figure 3b). Then L linkers [35] connect the chains from the direction of perpendicular to the loop to furnish a 2D bipillared layer (Figure 3c).

The two pillars formed by L ligands and two OBA^{2-} ligands on one side of SBUs are topologically equivalent, so $Cd_2(CO_2)_2$ SBUs can be considered as 4-connected nodes, while OBA^{2-} and [40] L ligands are considered as linkers, the 2D network can be simplified to a **sql** net with point symbol $\{4^4 \cdot 6^2\}$. Furthermore, the packing diagram clearly shows that neighboring 2D networks are parallel with a separation of 7.32 Å and stack alternatively with ···AAA··· mode, as depicted in Figure 3d. These layers [45] overlap with one another, so there are 1D channels in the crystal structure with the size 16.983 × 22.939 $Å^2$ in diagonal (Figure 3e). The solvent-accessible volume is 433.9 $Å^3$ or 25.3% of the total unit cell volume and the channels are occupied by DMF and H_2O solvent molecules squeezed through PLATON program.
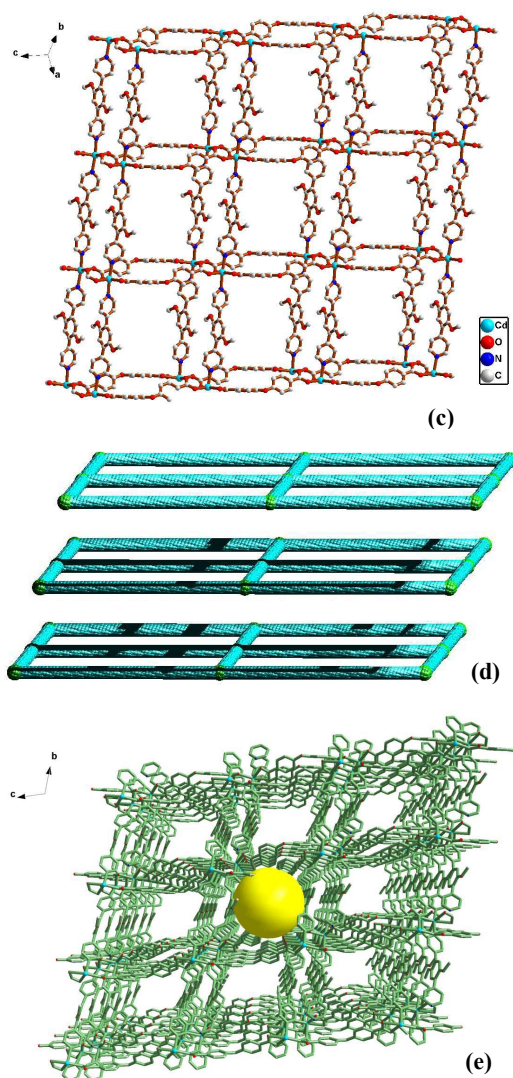

[50]

(a)

(b)

(c)

(d)

(e)

Figure 3. (a) Coordination environment of the Cd(II) ion in **4**. The hydrogen atoms and lattice solvent molecules are omitted for clarity (30% ellipsoid probability). Symmetry codes: #1 = x, y, 1+ z; #2 = 2 − x, 1 − y, − z; (b) An infinite 1D chain formed by Cd(II) cation centers and OBA^{2-} ligands with a loop; (c) A 2D bipillared layer in **4**; (d) Topological representation of AAA parallel stacking mode of the 2D sheets in **4**; (e) Central projection of 1D channels in the crystal structure of **4**.

Structural diversities for different metal centers

From the crystal structures of the four complexes discussed above, we can see that the choice of the metal ions will lead to structural diversity in assembly process. As summarized in Figure 4, three kinds of coordination geometries resulted, depending on the different metal centers, namely 4-coordinating tetrahedron in Co, Zn complexes, 6-coordinating octahedron in Ni complex and 6-coordinating bridging octahedron in Cd complex.

Since all complexes were assembled with the same ligands, same solvent systems under the same temperature, the assembly process is undoubtedly directed by the metal effect which should include three aspects: (i) metal ionic radii, (ii) electronic configurations of metal ions, and (iii) ligand conformation confined by metal. The ionic radii of the divalent metals are in the order 0.69, 0.72, 0.74, and 0.97 Å for Ni^{2+}, Co^{2+}, Zn^{2+}, and

Cd^{2+}, respectively [15] (Figure 4). Except for the smallest Ni^{2+} ion, an expectable coordination tendency is the smaller metal centers Co^{2+} and Zn^{2+} favor lower coordination number of four, while the larger metal center Cd^{2+} prefers a higher coordination number of six. However, different metal ions usually have preferential coordination geometry depending on their electronic configurations (d^7 for Co^{2+}, d^8 for Ni^{2+}, d^{10} for Zn^{2+} and Cd^{2+}). According to the ligand field theory,[16] the fully filled d^{10} (Cd^{2+}) metal ions take little contribution from the ligand coordination, and therefore prefer a flexible coordination geometry to accommodate as many donor atoms as possible. This is consistent with the observation of the two distorted 6-coordinating octahedrons bridged by two –OCO– groups for Cd complex. In contrast, the d^8 (Ni^{2+}) metal ion displays a strong preference to adopt an octahedral geometry due to the gain of the maximum ligand field stabilization energy. This obviously accounts for why the smallest Ni^{2+} ion favors 6-coordinating geometry in comparison with the 4-coordinating Co^{2+} and Zn^{2+} ions of slightly larger ionic radii. The tetrahedral geometry in Co^{2+} and Zn^{2+} complexes may be due to a balance between the electronic configurations of metal ions and ligand conformation. From table S3, the dihedral angles of OBA^{2-} ligands in Co^{2+} and Zn^{2+} complexes are 83.57 and 82.18°, respectively, which are obviously larger than the value of Cd^{2+} complex (53.95°), and similar with Ni^{2+} complex (88.13°). But the dihedral angles of L ligands in Co^{2+} (39.37°) and Zn^{2+} (37.43°) complexes are dramatically less than it in Ni^{2+} complex (65.05°), and similar with Cd^{2+} complex (33.08° for A↔C). The torsion angle differences between benzene rings of OBA^{2-} and L ligands in Co-/Ni-/Zn-/Cd-complexes may be caused by d-orbital splitting to gaining reasonable ligand field stabilization energy. A better expression of the stretching direction of the ligands is provided by topological simplification, as shown in the below of Figure 4, as well as the angles among the topological nodes.
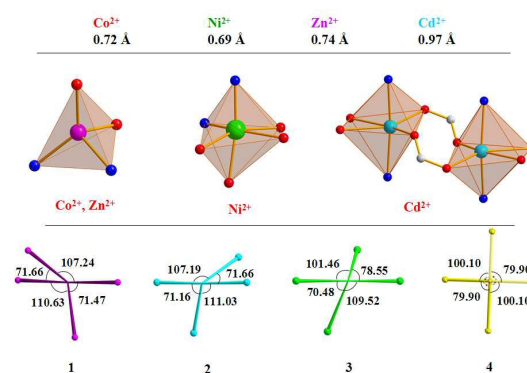
Figure 4. Representation of different coordination structures assembled from four different transition metal ions. The numbers below the cation symbols represent the cations' radii (Å). At the bottom of this graph represent the stretching direction of the ligands in complexes **1**–**4**, as well as the angles among the topological nodes.

X-ray powder diffraction results and thermogravimetric analyses

In order to check whether the crystal structures are truly representative of the bulk materials, the powder X-ray diffraction (PXRD) experiments for **1**–**4** were carried out at room

temperature. As shown in Figures S1–S4 (Supporting Information), the main peak positions of the simulated and experimental PXRD patterns are in agreement with each other. To estimate the stability of the crystal structures, their thermal behaviors were studied by TGA (Figure S15). For complex **1**, a weight loss of 5.68% from ambient temperature to 180 °C can be ascribed to the loss of the two water molecules (calcd 5.59%), which were removed by the SQUEEZE routine in PLATON and were obtained by element analyses. Then the TG curve presents a platform and the framework starts to decompose at 400 °C. The weight loss of 5.44% for compound **2** before 220 °C corresponds to the loss of lattice water molecules (calcd 5.38%), which were removed by the SQUEEZE routine in PLATON and were obtained by element analyses. Then the curve reaches a plateau until 420 °C, the sharply weightlessness represents the structure collapse. The TG curve of **3** shows a weightlessness 13.17% before 170 °C, is attributed to the loss of lattice DMF and H_2O molecules (calcd 13.32%), then the curve transforms into a plateau region. After 435 °C, a rapid weight loss is observed, which attributes to the decomposition of coordination framework. For complex **4**, the TG curve is similar with 3, there are two obvious weightlessness steps from 25 °C to 700 °C. From 25 °C to nearly 190 °C, the weight loss of 12.20% can be seen as the loss of solvent DMF and H_2O molecules (calcd 12.33%). The second step starts from 350 °C, the rapid weight loss can be seen as the burning of the organic ligands, at the same time accompanied by the collapse of the skeleton.

UV–visible spectra

The UV–vis absorption spectra of L ligand and complexes **1** and **3** were carried out in the crystalline state at room temperature (Figure S10a). The L ligand exhibits a wide absorption band in the range of 300–475 nm, which can be ascribed to π–π* transitions of the ligand. Complex **1** exhibits two absorption bands between 325 and 650 nm, one narrow band in the range of 325–425 nm can be ascribed to π–π* transitions of the ligand, the other wide band from 425 to 650nm can be considered as the spin–allowed d–d electronic transitions of the d^7 (Co^{2+}) cation.[17] Complex **3** has the wide absorption band at 510–740 nm can be due to the d–d electronic transitions of the d^8 (Ni^{2+}) cation. To explore the semiconductivity, the diffuse reflectance data is transformed into a Kubelka–Munk function [18] to obtain their band gaps (E_g). As shown in Figure S10a, the band gap of L ligand is approximately 2.86 eV, but the E_g value assessed from the steep absorption edge is 1.65 eV and 2.78 eV for **1**, 1.62 and 2.12 eV for **3**, respectively, which indicates that compound **1** and **3** are potential wide gap semiconductor materials.[19]

Luminescent properties

Complex **2** and **4** are insoluble in common organic solvents; so photoluminescence properties of **2** and **4** and free L ligand were investigated in the solid state at room temperature (Figure S11). The free L ligand exhibits an intense emission between 350 and 550 nm (λ_{max} = 428 nm upon excitation at 335 nm), which originated from charge transfer of the internal L ligand. The emission spectrum of complex **2** shows that the emission peaks center at 462 nm (λ_{ex} = 335 nm), which is red–shifted 34 nm. Compared with the emission spectrum of L, the origin of the broad and shifted emission band of complex **2** may be attributed to the contribution of ligand-to-metal charge transfer (LMCT). But for complex **4**, the emission peaks center at 425 nm (λ_{ex} =

350 nm) could be due to the charge transfer of the internal L ligand, a slightly blue-shifted 3 nm compared with L may be because of the coordination effect.[20] Furthermore, the emission decay lifetime of compound **2** and **4** were monitored. The luminescent decay curves (Figures S12–14) can be fitted with a double–exponential decay function. The results are summarized in Table S2. The emission lifetime value of complex **2** is higher than the corresponding value of L ligand, indicating that the emission of **2** can be attributed to both the charge transfer of the internal L ligand and LMCT. For complex **4**, the emission lifetime value is slightly lower than the value of L ligand, which may be ascribed to the effect of π*-π transitions between the carboxylate ligand and L ligand, and the magnitude of this influence is greater than the complex **2**.

Gas sorption properties.

The accessible volumes of the structures were estimated to be 11.3% for **1**, 12.3% for **2**, 19.7% for **3**, 25.3% for **4** of the total volume without the guest molecules in the pores by calculating from the single crystal structure with PLATON/SOLV. Before gas sorption experiments, the framework structural integrity of compounds **1−4** was evaluated using PXRD studies. Four compounds can maintain their porous framework after activated, (see Figures S1-4), so we concentrated on the gas adsorption properties of these compounds. The sorption measurements, using N_2, CO_2 and CH_4 as the adsorptive gas, were carried out on the activated compounds. Activated frameworks **1** and **2** showed no adsorption of N_2. It can be seen that a spot of N_2 uptake was observed at 77 K for **3** and **4** in the low-pressure region, and only shows 14.41 cm^3/g and 29 cm^3/g at 1 atm, which exhibits type III sorption profiles, suggesting that only surface adsorption occurs (Figures 5).[21]

The CO_2 sorption isotherms of **1−4** measured at 273 and 295 K are represented in Figures 6 and S17. The adsorption and desorption branches of the compounds show a slight hysteresis, which could be attributed to the presence of intercrystalline voids. The gas sorption isotherms shows the CO_2 uptake of 22.51 cm^3/g for **1**, 19.35 cm^3/g for **2**, 16.46 cm^3/g for **3**, 32.35 cm^3/g for **4** at 273 K and 15.68 cm^3/g for **1**, 17.70 cm^3/g for **2**, 10.10 cm^3/g for **3**, 26.75 cm^3/g for **4** at 295 K. Compound **4** exhibits the highest adsorption for CO_2; it is due to its relative high internal surface areas, which could provide the opportunity for more CO_2 efficient packing in the pores. Besides, CH_4 adsorption measurement has been carried out at 273 K. As seen in Figure S18, the sorption amount of CH_4 is much less than CO_2, 5.73 cm^3/g for **1**, 8.62 cm^3/g for **2**, 3.35 cm^3/g for **3**, 12.01 cm^3/g for **4** at 273 K and 1 atm. The adsorption for CO_2 is higher than that for CH_4, with a molar ratio for CO_2 / CH_4 of 3.91 for **1**, 2.24 for **2**, 4.90 for **3**, 2.69 for **4**, highlighting these compounds are potential materials for selective separation of CO_2 / CH_4.

Except that the distinct difference of adsorption capacity CO_2 / N_2 or CO_2 / CH_4 for compounds must be mainly associated with the smaller kinetic diameters of CO_2 (3.3 Å) than that of N_2 (3.64 Å) and CH_4 (3.80 Å), the Quadrupole Moment of CO_2 (-1.4×10^{-39} Cm^2) is the important factor that affect the distinct difference of adsorption capacity.[22] Though compound **3** has the larger accessible volumes (19.7%) than **1** (11.3%) and **2** (12.3%), the CO_2 sorption amount is the lowest in these four compounds, which could be the influence of the center metal of their structures. The difference of selective adsorption of CO_2 over

CH$_4$ among these four compounds may be partly because of the different interaction between the gases and the open metal sites.
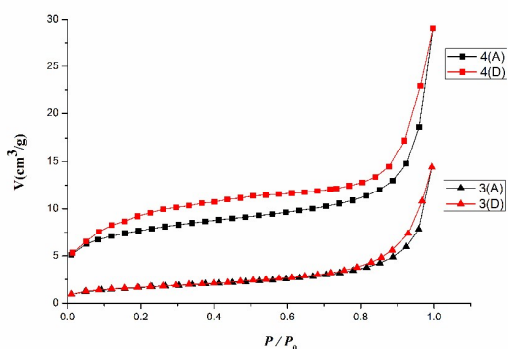

Figure 5. N$_2$ adsorption isotherms for **3** (triangle) and **4** (square) at 77 K. Black and red colour represent adsorption and desorption, respectively.
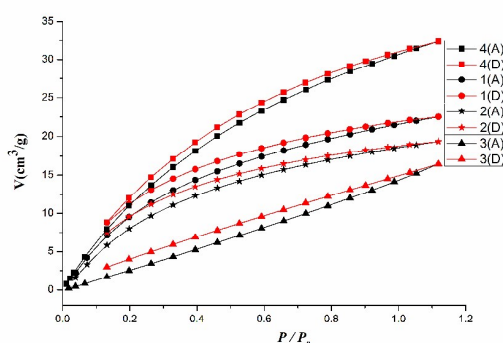

Figure 6. CO$_2$ sorption isotherms for **1** (circle), **2** (star), **3** (triangle) and **4** (square) at temperature 273 K. Black and red colour represent adsorption and desorption, respectively.

Conclusions

In summary, four coordination polymers with same ligands have been synthesized and characterized under the same solvent systems and same temperature. Based on different metal ionic radii and their electronic configurations, as well as ligand conformation confined by metal, these complexes exhibit interesting structural diversities. Complexes **1** and **2** with tetrahedral coordination centers present 3D unprecedented **hxg-d-4-Cccm** nets, **3** and **4** with octahedral coordination centers show 4-connected **sql** nets. These structural diversities led to their different properties. UV–visible spectra of **1** and **3** indicate the nature of semiconductivity. The strong fluorescence emission and long emission lifetime of **2** and **4** display them as promising fluorescent material. Gas adsorption properties indicate that these compounds are potential materials for adsorptive separation of CO$_2$ over N$_2$ and CO$_2$ over CH$_4$. Our work is underway to study that more materials with fascinating structures and interesting potential properties based on different metal centers.

Acknowledgments

References

1   a) X. Zhao, X. H. Bu, T. Wu, S. T. Zheng, L. Wang, P. Y. Feng, *Nat. Commun.*, 2013, **4**, 2344; b) R. E. Morris, X. H. Bu, *Nat. Chem.*, 2010, **2**, 353; c) S. M. Cohen, *Chem. Sci.* 2010, **1**, 32; d) R. Sessoli, A. K. Poweell, *Coord. Chem. Rev.*, 2009, **253**, 2328.

2   a) B. Li, H. M. Wen, H. L. Wang, H. Wu, M. Tyagi, T. Yildirim, W. Zhou, B. L. Chen, *J. Am. Chem. Soc.*, 2014, **136**, 6207; b) S. Pullen, H. H. Fei, A. Orthaber, S. M. Cohen, S. Ott, *J. Am. Chem. Soc.*, 2013, **135**, 16997; c) M. Mauro, K. C. Schuermann, R. Pretot, A. Hafner, P. Mercandelli, A. Sironi, L. D. Cola, *Angew. Chem., Int. Ed.*, 2010, **49**, 1222.

3   a) H. Furukawa, K. E. Cordova, M. O'Keeffe, O. M. Yaghi, *Science*, 2013, **341**, 974; b) K. Ohara, Y. Inokuma, M. Fujita, *Angew. Chem., Int. Ed.*, 2010, **49**, 5507; c) K. Oisaki, Q. W. Li, H. Furukawa, A. U. Czaja, O. M. Yaghi, *J. Am. Chem. Soc.*, 2010, **132**, 9262.

4   a) H. Sato, W. Kosaka, R. Matsuda, A. Hori, Y. Hijikata, R. V. Belosludov, S. Sakaki, M. Takata, S. Kitagawa, *Science*, 2014, **343**, 167; b) J. S. Mugridge, R. G. Bergman, K. N. Raymond, *Angew. Chem., Int. Ed.*, 2010, **49**, 1; c) M. Wang, Y. R. Zheng, K. Ghosh, P. J. Stang, *J.Am. Chem. Soc.*, 2010, **132**, 6282; d) S. Mirtschin, A. Slabon-Turski, R. Scopelliti, A. H. Velders, K. Severin, *J. Am. Chem. Soc.*, 2010, **132**, 14004.

5   a) L. J. Liu, K. Konstas, M. R. Hill, S. G. Telfer, *J. Am. Chem. Soc.*, 2013, **135**, 17731; b) Y. N. Guo, G. F. Xu, P. Gamez, L. Zhao, S. Y. Lin, R. P. Deng, J. K. Tang, H. J. Zhang, *J. Am. Chem. Soc.*, 2010, **132**, 8538; c) R. A. Layfield, J. J. W. McDouall, S. A. Sulway, F. Tuna, D. Collison, R. E. P. Winpenny, *Chem. Eur. J.*, 2010, **16**, 4442.

6   a) M. E. Schweinefuss, S. Springer, I. A. Baburin, T. Hikov, K. Huber, S. Leoni, M. Wiebcke, *Dalton Trans.*, 2014, **43**, 3528; b) J. H. Li, S. C. Meng, J. F. Zhang, Y. L. Song, Z. P. Huang, H. J. Zhao, H. Y. Wei, W. J. Huang, M. P. Cifuentes, M. G. Humphrey, *CrystEngComm.*, 2012, **14**, 2787; c) J. P. Zhang, X. C. Huang, X. M. Chen, *Chem. Soc. Rev.*, 2009, **38**, 2385.

7   X. Q. Liang, X. H. Zhou, C. Chen, H. P. Xiao, Y. Z. Li, J. L. Zuo, X. Z. You, *Cryst. Growth Des.*, 2009, **9**, 1041.

8   Y. Qi, F. Luo, Y. Che, J. Zheng, *Cryst. Growth Des.*, 2008, **8**, 606.

9   a) B. Y. Li, Y. M. Zhang, G. H. Li, D. Liu, Y. Chen, W. W. Hu, Z. Shi, S. H. Feng, *CrystEngComm.*, 2011, **13**, 2457; b) Y. Ma, A. L. Cheng, J. Y. Zhang, Q. Yue, E. Q. Gao, *Cryst. Growth Des.*, 2009, **9**, 867; c) Y. Gong, W. Tang, W. Hou, Z. Y. Zha, C. W. Hu, *Inorg. Chem.*, 2006, **45**, 4987.

10   L. Bain, S. Bullock, L. Harding, T. Riis-Johannessen, G. Midgley, C. R. Rice, M. Whitehead, *Chem. Commun.*, 2011, **13**, 2457.

11   Y. Liu, M. Pan, K. Li, C. Yan, Y. Shen, C. Y. Zhao, W. Wang, C. Y. Su, *Cryst. Growth Des.*, 2011, **11**, 4876.

12   C. L. Zhang, M. D. Zhang, L. Qin, H. G. Zheng, *Cryst. Growth Des.*, 2014, **14**, 491.

13   Spek, A. L. PLATON; The University of Utrecht: Utrecht, The Netherlands, 1999.

14   a) F. Luo, Z. Z. Yuan, X. F. Feng, R. B. Stuart, J. Q. Li, M. B. Luo, S. J. Liu, W. Y. Xu, G. M. Sun, Y. M. Song, H. X. Huang, X. Z. Tian., *Cryst. Growth Des.*, 2012, **12**, 3392; b) P. C. Cheng, M. H. Wu, M. Y. Xie, W. J. Huang, H. Y. He, T. T. Wu, Y. C. Lo, D. M. Proserpio, J. D. Chen, *CrystEngComm.*, 2013, **15**, 10346.

15   N. Y. Chen, W. C. Lu, J. Yang, G. Z. Li, Support Vector Machine in Chemistry: World Scientific Publishing Co. Pte. Ltd., Singapore, 2004.

16   H. L. Schläfer, G. Gliemann, Basic Principles of Ligand Field Theory: Wiley Interscience: New York, 1969.

17   a) D. Sarma, K. V. Ramanujachary, S. E. Lofland, T. Magdaleno, S. Natarajan, *Inorg. Chem.*, 2009, **48**, 11660; b) M. Tonigold, Y. Lu, A. Mavrandonakis, A. Puls, R. Staudt, J. Möllmer, J. Sauer, D.

Volkmer, *Chem. Eur. J.*, 2011, **17**, 8671; c) B. K. Tripuramallu, P. Manna, S. N. Reddy, S. K. Das, *Cryst. Growth Des.*, 2012, **12**, 777.

18   P. Kubelka, F. Z. Munk, *Tech. Phys.*, 1931, **12**, 593.

19   a) M. Alvaro, E. Carbonell, B. Ferrer, F. X. L. Xamena, H. Garcia, *Chem. Eur. J.*, 2007, **13**, 5106; b) K. Maeda, M. Higashi, D. Lu, R. Abe, K. Domen, *J. Am. Chem. Soc.*, 2010, **132**, 5858; c) F. Hu, Q. G. Zhai, S. N. Li, Y. C. Jiang, M. C. Hu, *CrystEngComm.*, 2011, **13**, 414.

20   a) S. Wang, *Coord. Chem. Rev.*, 2001, **215**, 79; b) L. L. Wen, D. B. Dang, C. Y. Duan, Y. Z. Li, Z. F. Tian, Q. J. Meng, *Inorg. Chem.*, 2005, **44**, 7161.

21   a) M. S. Chen, M. Chen, T.-a. Okamura, W. Y. Sun, N. Ueyama, *Microporous Mesoporous Mater.*, 2011, **139**, 25; b) K. S. W. Sing, *Pure Appl. Chem.*, 1982, **54**, 2201.

22   (a) D. W. Beck, *Zeolite Molecular Sieves*; Wiley & Sons: New York, 1974; (b) A. Bhunia, V. Vasylyeva, C. Janiak, *Chem. Commun.*, 2013, **49**, 3961; (c) S. S. Mondal, S. Dey, I. A. Baburin, A. Kelling, U. Schilde, G. Seifert, C. Janiak, H. J. Holdt, *CrystEngComm*, 2013, **15**, 9394.

Journal Name

ARTICLE TYPE

Table 1. Crystal data and structural refinements parameters of complexes **1**–**4**.

Complex	**1**	**2**	**3**	**4**
Empirical formula	$C_{32}H_{28}N_2O_9Co$	$C_{32}H_{28}N_2O_9Zn$	$C_{35}H_{33}N_3O_9Ni$	$C_{35}H_{33}N_3O_9Cd$
Formula weight	643.46	649.9	698.34	751.93
Crystal system	Monoclinic	Monoclinic	Triclinic	Triclinic
Space group	$C2/c$	$C2/c$	$P\bar{1}$	$P\bar{1}$
a / Å	25.3160(17)	25.434(7)	11.5007(11)	9.317(3)
b / Å	13.9919(10)	13.976(4)	11.7623(11)	12.722(4)
c / Å	17.8674(12)	17.825(5)	13.8198(13)	15.451(4)
α / °	90.00	90.00	70.8350(10)	108.632(4)
β / °	100.3550(10)	99.875(5)	65.6940(10)	97.755(4)
γ / °	90.00	90.00	76.9930(10)	91.789(4)
V / Å^3	6225.9(7)	6242(3)	1600.5(3)	1714.2(9)
Z	8	8	2	2
D_{calcd} / g cm^{-3}	1.296	1.306	1.445	1.281
μ / mm^{-1}	0.599	0.834	0.668	0.680
$F(000)$	2524	2548	726	768
θ min-max / °	1.64 , 27.53	1.95, 28.34	1.68, 26.37	1.41, 25.00
Tot., uniq. data	27865, 7148	21030, 7721	12668, 6421	11582, 5790
R(int)	0.0358	0.0457	0.0472	0.0904
Nref, Npar	7148, 381	7721, 381	6421, 437	5790, 381
$R1$, $wR2$ [I > 2σ(I)]	0.0379, 0.1082	0.0411, 0.1015	0.0517, 0.1559	0.0727, 0.1731
GOF on F^2	1.047	1.005	1.016	1.003
Min. and max resd dens (e·Å^{-3})	-0.251, 0.248	-0.395, 0.398	-1.002, 0.955	-2.071, 1.476

$R_1=\Sigma||F_o|-|F_c||/\Sigma|F_o|$; $wR_2=\{\Sigma[w(F_o^2-F_c^2)^2]/\Sigma[w(F_o^2)^2]\}^{1/2}$; where $w=1/[\sigma^2(F_o^2)+(aP)^2+bP]$,$P=(F_o^2+2F_c^2)/3$.

5

10

For Table of Contents Use Only

Diverse Structures of Metal – Organic Frameworks Based on Different Metal Ions: Luminescence and Gas Adsorption Properties

Chuan-Lei Zhang, Ling Qin, Zhen-Zhen Shi and He-Gen Zheng[*]

Diverse structures of metal–organic frameworks induced by different metal ions under solvothermal conditions exhibit different topological characteristics and spectral properties.